Water-Soluble Flexible Organic Frameworks That Include and Deliver Proteins

Jia-Le Lin,† Ze-Kun Wang,† Zi-Yue Xu,† Lei Wei,‡ Yun-Chang Zhang,*,† Hui Wang,† Dan-Wei Zhang,† Wei Zhou,*,† Yue-Biao Zhang,‡ Yi Liu,*,§ and Zhan-Ting Li*,†

†Department of Chemistry, Shanghai Key Laboratory of Molecular Catalysis and Innovative Materials, Fudan University, 2205 Songhu Road, Shanghai 200438, China

‡School of Physical Science and Technology, ShanghaiTech University, Shanghai 201210, China

§The Molecular Foundry, Lawrence Berkeley National Laboratory, One Cyclotron Road, Berkeley, California 94720, United States

ABSTRACT: Four water-soluble hydrazone-based three-dimensional (3D) flexible organic frameworks **FOF-1~4** have been synthesized from a semi-rigid tetracationic tetraaldehyde and four flexible dihydrazides. ^{1}H NMR spectroscopy indicated the quantitative formation of **FOF-1~4** in D_2O, while dynamic light scattering experiments revealed that, depending on the concentration, these porous frameworks display hydrodynamic diameters ranging from 50 nm to 120 nm. The porosity of the frameworks is confirmed by ethanol vapor adsorption experiments of the solid samples as well as the high loading capacity for a 2.3 nm-sized porphyrin guest in water. The new water-soluble frameworks exhibit low cytotoxicity and form inherent pores with diameters of 5.3 nm or 6.7 nm, allowing rapid inclusion of proteins such as bovine serum albumin, green and orange fluorescent proteins, and efficient delivery of the proteins into normal and cancer cells. Flow cytometric analysis reveals percentages of the delivered cells up to 99.8%.

INTRODUCTION

Porous polymers have attracted the interest of chemists for decades due to their great potential for applications in separation, catalysis, inclusion and delivery.[1–4] Three-dimensional (3D) polymers are structurally ideal for the design of porous materials due to their intrinsic tendency of forming networks. Since the pioneering theoretical study by Flory in 1940s,[5] numerous 3D polymers have been prepared from flexible monomers,[4,6,7] and several structures have been exploited as swellable self-healing materials.[8–10] Water-soluble 3D polymers with inherent nanoscale pores are desirable for the inclusion and delivery of biomacromolecules such as DNAs and proteins, thus hold great promises as biocompatible materials for both diagnostic and therapeutic purposes.[11-13] The design and synthesis of this family of polymers, however, remains an underdeveloped area.

Dynamic covalent chemistry provides a robust foundation for the synthesis of thermodynamically controlled macromolecular and supramolecular targets.[14–23] To date, attempts to prepare porous polymers using this strategy have generally focused on the construction of crystalline covalent organic frameworks under solvothermal conditions.[24–31] However, to the best of our knowledge, examples of water-soluble polymeric frameworks that possess nanoscale pores for efficient guest encapsulation have not been reported. Herein we describe the synthesis of a new kind of flexible organic frameworks through quantitative formation of hydrazone bonds in water by balancing the rigidity and flexibility of the molecular components. We demonstrate that the new water-soluble frameworks possess good biocompatibility and large pores of 5.4 or 6.7 nm-aperture, which allows in situ protein inclusion and efficient intracellular delivery.

RESULTS AND DISCUSSION

Synthesis and Characterization Using ^{1}H NMR and Infrared Spectroscopy. A hydrazine and an aldehyde react to form hydrazone in water,[15,16] which can be promoted to be quantitative through the multivalency principle.[32,33] We prepared water-soluble, semi-rigid tetraaldehyde **T1**[34] and flexible biacylhydrazines **L1**~**L4**, and studied their reactions for the preparation of hydrazone-based 3D polymers. The reactions were first investigated in D_2O using ^{1}H NMR spectroscopy by keeping the 1:2 stoichiometric ratio (Scheme 1). At [**T1**] = 2.4 mM, the reactions proceeded quantitatively at room temperature under the catalysis of hydrochloric acid, as confirmed by the observation that the diagnostic O=C*H* signal of **T1** at ~9.9 ppm vanished completely after about 30 minutes (Figures S1-S4). ^{1}H NMR spectra of all the resulting products were broad, suggesting the formation of hydrazone-based polymeric species. We termed this new family of polymers as flexible organic frameworks (**FOF-1~4**) as they were synthesized from flexible building blocks through dynamic hydrazone bonds and maintained inherent nanoscale pores. Increasing the temperature to 90 °C caused the occurrence of a weak C*H*O peak in the ^{1}H NMR spectrum of **FOF-1**, which indicated partial hydrolysis of the hydrazone bond (Figure S5). However, upon cooling to room temperature, this signal vanished again, which supported that the aldehyde transformed back to hydrazone. The ^{1}H NMR spectrum of **FOF-1** prepared from the reaction of **T1** (1.2 mM) and **L1** (2.4 mM) was nearly identical to that of the solution of the same concentration obtained by diluting a more concentrated solution ([**T1**] = 2.4 mM), which well reflected the dynamic feature of the hydrazone bond. Decreasing the concentration to 0.6 mM (based on [**T1**]) did not induce any C*H*O signals (Figures S6-S9), indicating that the hydrazone bonds remained intact in diluted solutions. Further ^{1}H NMR spectroscopic studies indicated that, after reaching equilibrium, the reaction of the

control compound 4-(4-benzylpyridin-4-yl)benzaldehyde (**M1**, 9.6 mM) and **L1** (4.8 mM) took place in 88% yield for the hydrazone bond formation (Figure S10). The higher hydrazone conversion rate in the case of **T1** suggested a positive multivalency effect, through which the hydrazone bonds of **FOF-1~4** stabilized each other to enable quantitative formation. The infrared spectrum of **FOF-1~4** showed that the stretching vibration of the aldehyde C=O bond of **T1**, centered at 1703 cm-1, disappeared completely (Figures S11-S14), consistent with the quantitative formation of hydrazone bonds.

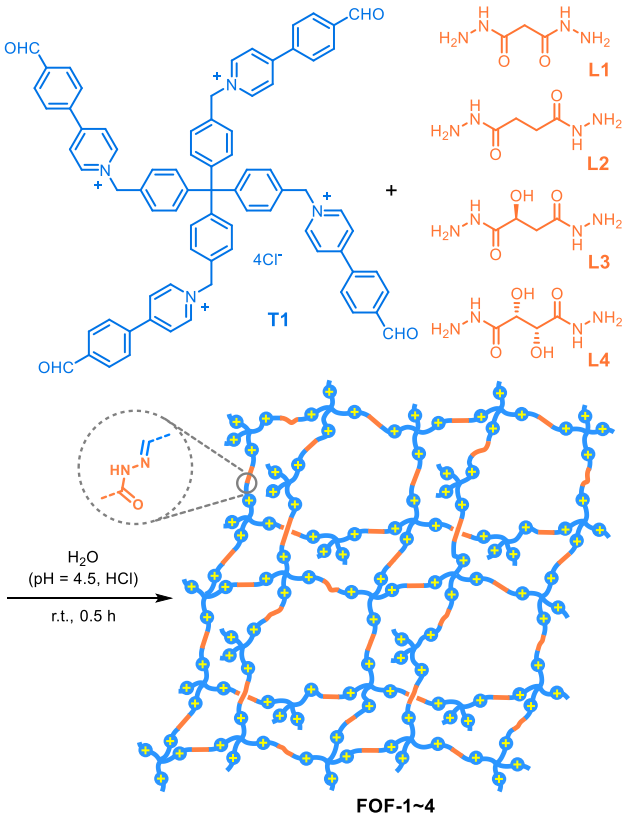

Scheme 1. Synthesis of hydrazone-based flexible organic frame-works FOF-1~4 from the condensation reactions of T1 and L1~L4 in water. The polymeric framework is expected to be flexible and dynamic in solution.

Dynamic Light Scattering (DLS) and Zeta Potential Measurements. The DLS profiles of the solutions of **FOF-1~4** revealed that, at [**T1**] = 2.4 mM, the solutions gave rise to a hydrodynamic diameter (D_H) of 122, 91, 122 and 106 nm, respectively (Figures 1 and S15). Similar results were obtained after the solutions were left to stand for three months, which supported the high stability of the homogeneous frameworks. In contrast, the solution of **T1** at 2.4 mM afforded a much smaller D_H of about 10 nm (Figure 1), which reflected intermolecular stacking of the hydrophobic 4-phenylpyridinium units. The D_H values of the frameworks decreased with the decrease of the concentration (Figures 1 and S15). However, even at [**T1**] = 0.1 mM, the solutions still afforded D_H ranging from 12 nm to 38 nm. To study the influence of pH on the D_H change of the frameworks, we used NaOH to adjust the above solution of **FOF-1** ([**T1**] = 2.4 mM) to pH = 7.3 and then diluted the solution to [**T1**] = 0.1 mM. The dilute solution was left to stand for 24 h and then subjected to the DLS measurement, which afforded a D_H of 91 nm (Figure S15). This value was considerably larger than that (38 nm) obtained for the solution of the identical concentration at pH = 4.5 (Figure 1). Clearly, the exchange of the hydrazone bonds in the dynamic polymers became significantly slower in the weakly alkaline medium, which was crucially important for the encapsulation and delivery of proteins (vide infra). The zeta potential of **FOF-1~4** at pH = 7 was determined to be 46.2, 25.3, 23.9 and 38.6 mV (Table 1), respectively, which indicated that all of the frameworks possessed a positively charged surface.

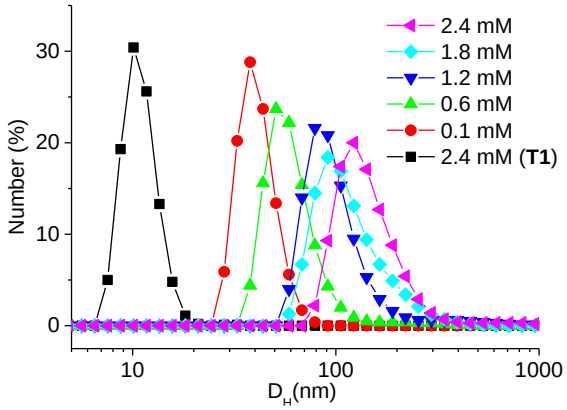

Figure 1. The DLS profile of FOF-101 and T1 at different concentrations in water at 25 °C at pH = 4.5 adjusted with hydrochloric acid. The solutions were left to stand for 24 h before being measured.

Table 1. Zeta potential of the flexible frameworks, proteins and their mixtures in water[a]

		FOF-1	FOF-2	FOF-3	FOF-4
	□	+46.2	+25.3	+23.9	+38.6
BSA	–17.7	+4.90	+12.2	+15.2	+11.4
GFP	–35.5	+19.4	+21.1	+15.4	+25.8
OFP	–26.2	+22.5	+12.6	+8.80	+23.0

[a][**FOF-1~4**] = 3 μg/mL, [BSA] = 6 μg/mL, [GFP] = 2 μg/mL and [OFP] = 2 μg/mL.

Molecular Modelling and Porphyrin Guest Inclusion. Molecular modelling studies revealed that the aldehyde units of **T1** could not condense with either of **L1-L4** to form simple 1 + 1 macrocycles. By assuming an ideal condensation process and all the aliphatic chains adopted a fully extended conformation, **FOF-1~4** would form a dynamic 3D diamondoid framework. The aperture of the cyclohexane-like pore formed through 6 + 6 condensation of the two components was calculated to be about 5.3 nm for **FOF-1** and 6.7 nm for **FOF-2~4** (Figure S16).[35] To test if these dynamic covalent polymers formed inherent pores, guest inclusion studies were performed. Powders of **FOF-1** and **FOF-4** were prepared by evaporating their respective solutions under reduced pressure. Once dried, the powders remained insoluble at room temperature within a 24 h period. The powders were then exposed to a solution of the rigid 4,4',4",4'"-porphyrin-5,10,15,20-tetrabenzoate (PTB, as sodium salt), which has a width of ~2.3 nm, and the guest adsorption was followed using UV-vis spectroscopy. Adding 1.1, 2.2, 4.4 or 6.6 mg of the two powders, which corresponded to 1, 2, 4 and 6 equiv. of the cation units relative to the anion of PTB, to the aqueous solution of PTB (0.25 mM, 3 mL) led to significant adsorption of the dye, as indicated by rapid fading

of the solution color and the color change of the powder from light yellow to purple (Figure S17). By recording the absorbance of PTB before and after the adsorption, we determined that 61%, 71%, 88% and 100% of PTB was adsorbed by **FOF-1** and 66%, 75%, 90% and 100% of PTB was adsorbed by **FOF-4** at the four different equivalencies. The facts that 1 equiv of the framework realized adsorption of over 60% PTB supported that, instead of adsorbing the guests just on the surface, the framework formed inherent pores to include the porphyrin guests. Dialysis experiments (molecular weight cut-off: 1000 Da) for the mixture solution of PTB (MW: 878) and **FOF-1~4** (anion/cation molar ratio: 1:2) in water showed that the frameworks nearly completely prevented PTB from leaking (<1.5%) after three days (Figure S18), further confirming the inclusion of the guests in the frameworks which suppressed the dialysis of the guests.

Ethanol Vapor Adsorption Isotherm and Transmission Electron Microscopic (TEM) Measurements. To study the porosity of the polymeric frameworks, we further collected the vapor adsorption isotherms of ethanol for the solid samples of **FOF-1~4** at 25 °C (Figure S19). The samples were obtained by the lyophilization of the neutral aqueous solutions. All the four samples displayed a similar uptake pattern. At P/P_0 = 0.92, 0.96, 0.97 and 0.97, their pore volumes were calculated to be 0.32, 0.42, 0.26, and 0.26 $cm^{-3} \cdot g^{-1}$, respectively. The values are comparable with those reported for several covalent organic frameworks.[36–38] The TEM images of the solid samples of **FOF-1~4** revealed the formation of amorphous aggregates (Figure S20), which reflected the flexibility of the porous frameworks.

Cytotoxicity and Protein Inclusion and Delivery. The cytotoxicity of **FOF-1~4** was then evaluated with ana-1, hepg2, lovo and skov3 cell lines using the Cell Counting Kit-8 (CCK-8) assay (Figure S21). At the concentration of 30 μg of the frameworks, all 16 tested cell lines maintained ≥85% viability. At the concentration of 60 μg, 15 cell lines still maintained 75% viability, with one case having 71.5% viability— **FOF-4** for ana-1 cell line. These preliminary results showed that the cytotoxicity of the frameworks was reasonably low. Their inclusion of proteins was thus further investigated. We chose BSA, GFP and OFP to test this potential. BSA and GFP have dimensions of 4 nm × 4 nm × 14 nm and 3.4 nm × 3.4 nm × 4.4 nm, respectively, whereas OFP has a barrel structure similar to that of GFP, but a different fluorescent dye in the barrel. Fluorescent experiments for **FOF-1** revealed that the framework efficiently quenched the fluorescence of fluorescein isothiocyanate (FITC)-marked BSA, GFP and OFP (Figure S22). In contrast, control compound **C1** (see Supporting Information for the structure) displayed much lower quenching ability (Figure S23). These observations provided the first evidence that the proteins could also be included into the interior of **FOF-1**. The quenching was also time-independent, which supported a quick, diffusion-determined process.

Isothermal calorimetric (ITC) experiments were further conducted for **FOF-1** and BSA, GFP and OFP (Figure S24), from which the apparent binding constants for the complexation between its **T1** units and the proteins were determined to be 2.7 × 10_4, 8.1 × 10_6 and 6.9 × 10_7 M^{-1}, respectively. This treatment of the binding between **FOF-1** and the proteins was adopted given that the polymeric framework had no accurate molecular weight and the proteins had no specific and fixed binding sites, whereas the accurate concentrations of the **T1** units in **FOF-1** and the proteins were available. Assuming that all the **T1** units had identical binding affinities towards one protein, we could derive the apparent binding constants from the ITC measurements, which, to some extent, quantitatively reflected the binding ability of the framework towards the three proteins.[39,40] Although no further experiments were conducted for another three frameworks, given their increased pore size, it was rational to assume that they possessed similar ability for including the proteins.

All three proteins gave rise to a negative zeta potential (Table 1), whereas their mixtures with the frameworks all exhibited a positive zeta potential ranging from 4.9 mV to 25.8 mV. These observations supported strong interactions between the frameworks and the proteins, which might occur through simple surface-to-surface contact or the inclusion of the proteins by the frameworks. As confocal laser microscopy imaging and flow cytometric experiments (vide infra) revealed that the frameworks exhibited good ability of cellular delivery of the proteins, it is rational to propose that the proteins were included inside the frameworks. Moreover, if the interactions took place only on the surfaces of the porous frameworks, one might expect that the mixtures would give rise to negative zeta potentials because the amounts of the negatively charged proteins were large enough to cover the frameworks. The solution of the three proteins exhibited very comparable circular dichroism signals in the absence and presence of the frameworks **FOF-1** and **FOF-4** (Figures S25 and S26), which indicated that the included proteins in the frameworks maintained their secondary and tertiary structures.

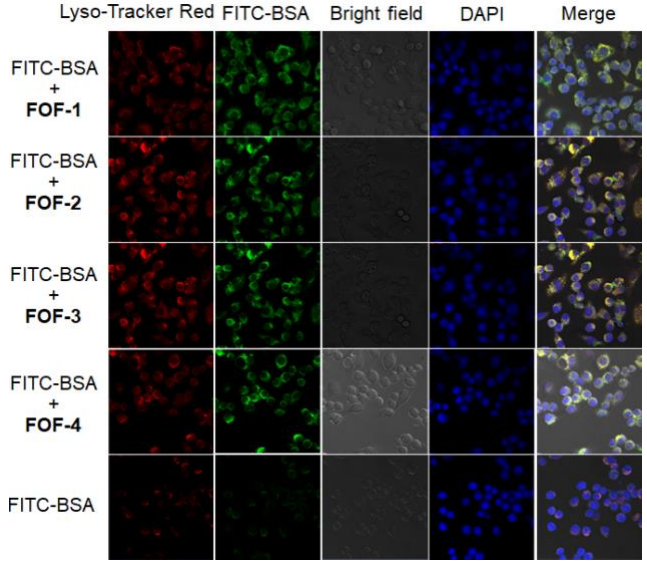

Figure 2. Confocal laser microscopic images of ana-1 cells after incubation for 16 h with FITC-BSA (6 μg) in the presence or absence of **FOF-1~4** (12 μg). The lysosomes and nuclei were stained with Lyso-Tracker Red (red) and DAPI (blue), respectively.

The delivery of FITC-BSA by the frameworks was then investigated, first with ana-1 cell lines, by staining the lysosomes with Lyso-Tracker Red and the nuclei with 4',6-diamidino-2-phenylindole (DAPI). After incubation with FITC-BSA⊂**FOF-1~4** for 16 h, the cells were subjected to confocal laser scanning microscopy (CLSM) (Figure 2). It was found that, for all four samples, the fluorescence signal of the FITC marker was very clear and highly overlapped with that of Lyso-Tracker Red-stained lysosomes and DAPI-stained nuclei. In the absence of the frameworks, no fluorescence of the FITC

marker was observed for free FITC-BSA. These observations clearly supported that all four frameworks delivered BSA into the ana-1 cells. Further CLSM experiments revealed that the four frameworks could also realize the delivery of GFP or OFP into the ana-1 cells (Figures S27 and S28). As all the water-soluble frameworks enabled cellular delivery of the proteins, we further tested the capacity of **FOF-1** for delivering FITC-BSA into hepg2, skov3 and lovo cancer cells through CLSM experiments, which also confirmed the capacity for all the cancer cell lines (Figures S29-S31). CLSM experiments with control **C1** of the same amount revealed that **C1** displayed no ability to deliver the proteins into the cells (Figure S32).

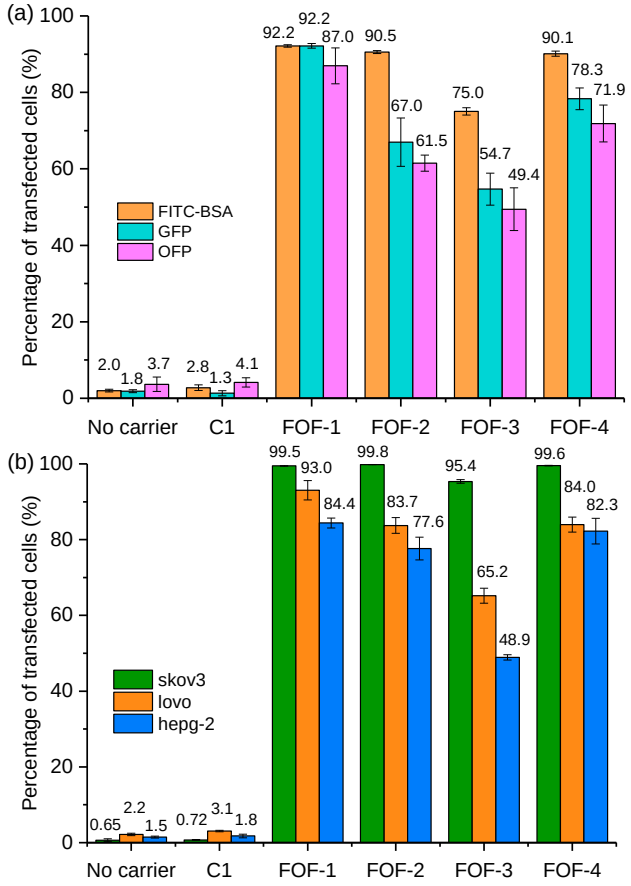

Figure 3. Delivery experiments of (a) FITC-BSA (6 μg/mL), GFP (2 μg/mL) and OFP (2 μg/mL) by **C1** (12 μg/mL) or **FOF-1~4** (12 μg/mL) into ana-1 cell lines, and (b) FITC-BSA (6 μg/mL) by **C1** (12 μg/mL) or **FOF-1~4** (12 μg/mL) into skov3, hepg2 and lovo cancer cell lines after incubation in 3% FBS for 16 h at 37 °C.

Flow cytometry was further used to investigate the intracellular delivery of FITC-BSA, GFP and OFP by **FOF-1~4** to ana-1 cells (Figure 3a). For FITC-BSA, all four frameworks exhibited good to excellent delivery capacity (Figure S33). The percentage of the transfected cells (PTC) was determined in the range from 75.0% to 92.2%. Without the frameworks, FITC-BSA itself attained a PTC of 2.0%, which supported that the frameworks made an overwhelming contribution in the transfection of the FITC marker for the cells. The 1:2 weight ratio represented a large loading of the frameworks for FITC-BSA. When the amount of **FOF-1** was reduced to a 1:1 weight ratio, it still could realize PTC of 64.0% (Figure S34). All the frameworks could also deliver GFP and OFP (Figures S35 and S36), with PTC ranging from 54.7% to 92.2% or from 49.4% to 87%, respectively. The values were consistently lowered than the related value of BSA. However, without the frameworks, neither of proteins could significantly transfect the cells, as PTC was determined to as low as 1.8% or 3.7%). Among others, **FOF-1** displayed the largest delivery capacity.

The delivery capacity of **FOF-1~4** for FITC-BSA into skov3, hegp2 and lovo cancer cells was further evaluated using flow cytometry (Figures 3b and S37-S39). For skov3 cell lines, all the frameworks exhibited high delivery efficiency, with PTC being 95.4% to 99.8%. For lovo cell lines, **FOF-1**, **FOF-2** and **FOF-4** exhibited good delivery ability, with PTC ranging from 83.7% to 93.0%, whereas **FOF-3** achieved a modest activity (PTC = 65.2%). Concerning hepg2 cell lines, the delivery ability of the frameworks were generally lowered. Nevertheless, **FOF-1** and **FOF-4** still realized PTC of 84.4% and 82.3%, respectively. Flow cytometry experiments for **C1** also showed that this control compound did not possess the ability to deliver the three proteins into the four cells (Figure 3).

Finally, the pathway for the internalization of the protein-included frameworks was investigated with **FOF-1**. To this end, before **FOF-1** treatment, ana-1 cells were pretreated with five endocytosis inhibitors, including sucrose and chlorpromazine, which inhibit clathrin-mediated endocytosis; nystatin, which inhibits caveolae-mediated endocytosis; amiloride, which inhibits micropinocytosis; and Me-β-CD, which inhibits caveolae-mediated endocytosis. PTC values obtained for these pretreated cells were compared to that of the untreated ana-1 cells (Figure S40). It was found that amiloride inhibited the delivery to the largest extent, by 42% as compared with the non-treated cells, while others did not display apparent inhibition activity, which suggested that the endocytosis of the protein-included FOFs by the cells occurred predominantly via the mechanism of macropinocytosis.[41,42] BSA, GFP and OFP all bear a large number of hydrophobic side chains, and their isoelectric points are 4.7, 5.8 and 5.8, respectively. Thus, in the weakly alkaline media used for the intracellular delivery, their inclusion by polycationic **FOF-1~4** might be driven by both hydrophobic and electrostatic attractions, whereas the endocytosis of the protein-included frameworks by the studied cells might proceed in a mechanism similar to that established for other multicationic porous frameworks or polymers.[43–46]

CONCLUSION

In this study, we have demonstrated that water-soluble flexible organic frameworks with nano-scale pores can be prepared through the formation of dynamic hydrazone bonds from readily accessible cationic and hydrophilic precursors. The inherent porosity of the resulting dynamic covalent polymers has been realized through the introduction of a rigid tetraphenylmethane support, whereas multivalency induced by the tetratopic monomers allows for quantitative formation of hydrazone bonds and thus the formation of porous frameworks with sizes over 100 nm. The large pores of the flexible polymer frameworks possess both ionic and hydrophobic inner domains for the inclusion of different proteins for efficient intracellular delivery. The flexible porous organic frameworks represent a unique expansion of the emerging crystalline covalent organic frameworks which have been extensively investigated as solid-state materials. The combined features such as good water solubility and stability, controllable nanoscale sizes and easy preparation, may open the door to future applications as biocompatible soft materials.

ASSOCIATED CONTENT

Supporting Information

The Supporting Information is available free of charge on the ACS Publications website.

General methods, synthetic procedures, $_1$H NMR, IR, DLS, structural modelling, dialysis, cytotoxicity, fluorescence, ITC, CD, CLMS and flow cytometric profiles or images (PDF).

AUTHOR INFORMATION

Corresponding Authors

*yunchangzhang11@fudan.edu.cn
*zhouw@fudan.edu.cn
*yliu@lbl.gov
*ztli@fudan.edu.cn

ORCID

Yun-Chang Zhang: 0000-0002-0229-5899
Dan-Wei Zhang: 0000-0003-1244-1850
Wei Zhou: 0000-0001-7467-3628
Yue-Biao Zhang: 0000-0002-8270-1067
Yi Liu: 0000-0002-3954-6102
Zhan-Ting Li: 0000-0003-3954-0015

Notes

The authors declare no competing financial interest.

ACKNOWLEDGMENTS

Z.T.L. acknowledges funding from National Natural Science Foundation of China (21890732 and 21921003). We thank Shanghai Synchrotron Radiation Facility for providing BL16B1 and BL14B1 beamlines for conducting synchrotron X-ray-scattering and diffraction experiments. Part of the work is carried out as a user project at the Molecular Foundry, which is supported by the Office of Science, Office of Basic Energy Sciences, of the U.S. Department of Energy under Contract No. DE-AC02-05CH11231.

REFERENCES

(1) Wu, D.; Xu, F.; Sun, B.; Fu, R.; He, H.; Matyjaszewski, K. Design and preparation of porous polymers. *Chem. Rev.* **2012**, *112*, 3959–4015.

(2) Sun, Q.; Dai, Z.; Meng, X.; Xiao, F.-S. Porous polymer catalysts with hierarchical structures. *Chem. Soc. Rev.* **2015**, *44*, 6018–6034.

(3) Wu, J.; Xu, F.; Li, S.; Ma, P.; Zhang, X.; Liu, Q.; Fu, R.; Wu, D. Porous polymers as multifunctional material platforms toward task-specific applications. *Adv. Mater.* **2019**, *31*, 1802922.

(4) Zheng, C.; Zhu, J.; Yang, C.; Lu, C.; Chen, Z.; Zhuang, X. The art of two-dimensional soft nanomaterials. *Sci. China Chem.* **2019**, *62*, 1145–1193.

(5) Flory, P. J. Molecular size distribution in three-dimensional polymers. I. Gelation. *J. Am. Chem. Soc.* **1941**, *63*, 3083–3090.

(6) Kopeček, J; Yang, J. Hydrogels as smart biomaterials. *Polymer Int.* **2007**, *56*, 1078–1098.

(7) Wang, W.; Narain, R.; Zeng, H. Rational design of self-healing tough hydrogels: a mini review. *Front. Chem.* **2018**, *6*, 497.

(8) Bracco, S.; Piga, D.; Bassanetti, I.; Perego, J.; Comotti, A.; Sozzani, P. Porous 3D polymers for high pressure methane storage and carbon dioxide capture. *J. Mater. Chem. A* **2017**, *5*, 10328–10337.

(9) Postiglione, G.; Alberini, M.; Leigh, S.; Levi, M.; Turri, S. Effect of 3D-printed microvascular network design on the self-healing behavior of cross-linked polymers. *ACS Appl. Mater. Interfaces* **2017**, *9*, 14371–14378.

(10) Song, F.; Li, Z.; Jia, P.; Zhang, M.; Bo, C.; Feng, G.; Hu, L.; Zhou, Y. Tunable "soft and stiff", self-healing, recyclable, thermadapt shape memory biomass polymers based on multiple hydrogen bonds and dynamic imine bonds. *J. Mater. Chem. A* **2019**, *7*, 13400–13410.

(11) Reineke, T. M.; Raines, R. T.; Rotello, V. M. Delivery of Proteins and Nucleic Acids: Achievements and Challenges. *Bioconjugate Chem.* **2019**, *30*, 261–262.

(12) Liu, X.; Wu, F.; Ji, Y.; Yin, L. Recent Advances in Anti-cancer Protein/Peptide Delivery. *Bioconjugate Chem.* **2019**, *30*, 305–324.

(13) Wang, S.; Chen, Y.; Wang, S.; Li, P.; Mirkin, C. A.; Farha, O. K. DNA-Functionalized Metal-Organic Framework Nanoparticles for Intracellular Delivery of Proteins. *J. Am. Chem. Soc.* **2019**, 141, 2215–2219.

(14) Rowan, S. J; Cantrill, S. J.; Cousins, G. R L; Sanders, J. K M; Stoddart, J. F. Dynamic covalent chemistry. *Angew. Chem. Int. Ed. Engl.* **2002**, *41*, 898–952.

(15) Corbett, P. T.; Leclaire, J.; Vial, L.; West, K. R.; Wietor, J.-L.; Sanders, J. K. M.; Otto, S. Dynamic combinatorial chemistry. *Chem. Rev.* **2006**, *106*, 3652–3711.

(16) Roy, N.; Bruchmann, B.; Lehn, J.-M. DYNAMERS: dynamic polymers as self-healing materials. *Chem. Soc. Rev.* **2015**, *44*, 3786–3807.

(17) Reuther, J. F.; Dahlhauser, S. D.; Anslyn, E. V. Tunable orthogonal reversible covalent (TORC) bonds: dynamic chemical control over molecular assembly. *Angew. Chem. Int. Ed.* **2019**, *58*, 74–85.

(18) Liu, Y.; Jia, Y.; Wu, Q.; Moore, J. S. Architecture-controlled ring-opening polymerization for dynamic covalent poly(disulfide)s. *J. Am. Chem. Soc.* **2019**, *141*, 17075–17080.

(19) Jin, Y.; Wang, Q.; Taynton, P.; Zhang, W. Dynamic covalent chemistry approaches toward macrocycles, molecular cages, and polymers. *Acc. Chem. Res.* **2014**, *47*, 1575–1586.

(20) Ye, H.; Hai, Y.; Ren, Y.; You, L. Versatile dynamic covalent assemblies for probing π-stacking and chirality induction from homotopic faces. *Chem. Eur. J.* **2017**, *23*, 3804–3809.

(21) Zou, W.; Dong, J.; Luo, Y.; Zhao, Q.; Xie, T. Dynamic covalent polymer networks: from old chemistry to modern day innovations. Adv. Mater. 2017, 29, 1606100.

(22) Garcia, F.; Smulders, M. M. J. Dynamic covalent polymers. *J. Polym. Sci. A* **2016**, *54*, 3551–3577.

(23) Ji, S.; Xia, J.; Xu, H. Dynamic chemistry of selenium: Se-N and Se-Se dynamic covalent bonds in polymeric systems. *ACS Macro Lett.* **2016**, *5*, 78–82.

(24) Cote, A. P.; Benin, A. I.; Ockwig, N. W.; O'Keeffe, M.; Matzger, A. J.; Yaghi, O. M. Porous, crystalline, covalent organic frameworks. *Science* **2005**, *310*, 1166–1170.

(25) Ding, S.-Y.; Wang, W. Covalent organic frameworks (COFs). from design to applications. *Chem. Soc. Rev.* **2013**, *42*, 548–568.

(26) Feng, X.; Ding, X.; Jiang, D. Covalent organic frameworks. *Chem. Soc. Rev.* **2012**, *41*, 6010–6022.

(27) Bisbey, R. P.; Dichtel, W. R. Covalent organic frameworks as a platform for multidimensional polymerization. *ACS Central Sci.* **2017**, *3*, 533–543.

(28) Yuan, F.; Tan, J.; Guo, J. Assemblies of covalent organic framework microcrystals: multiple-dimensional manipulation for enhanced applications. *Sci. China Chem.* **2018**, *61*, 143–152.

(29) Kandambeth, S.; Dey, K.; Banerjee, R. Covalent organic frameworks: chemistry beyond the structure. *J. Am. Chem. Soc.* **2019**, *141*, 1807–1822.

(30) Lohse, M. S.; Bein, T. Covalent organic frameworks: structures, synthesis, and applications. *Adv. Funct. Mater.* **2018**, *28*, 1705553.

(31) Liang, R.-R.; Zhao, X. Heteropore covalent organic frameworks: a new class of porous organic polymers with well-ordered hierarchical porosities. *Org. Chem. Front.* **2018**, *5*, 3341–3356.

(32) Badjic, J. D.; Nelson, A.; Cantrill, S. J.; Turnbull, W. B.; Stoddart, J. F. Multivalency and cooperativity in supramolecular chemistry. *Acc. Chem. Res.* **2005**, *38*, 723–732.

(33) Li, X.-F.; Yu, S.-B.; Yang, B.; Tian, J.; Wang, H.; Zhang, D.-W.; Liu, Y.; Li, Z.-T. A stable metal-covalent-supramolecular organic framework hybrid: enrichment of catalysts for visible light-induced hydrogen production. *Sci. China Chem.* **2018**, *61*, 830–835.

(34) Wu, Y.-P.; Yang, B.; Tian, J.; Yu, S.-B.; Wang, H.; Zhang, D.-W.; Liu, Y.; Li, Z.-T. Postmodification of supramolecular organic

framework: visible-light-induced recyclable heterogeneous photocatalysis for reduction of azides to amines. *Chem. Commun.* **2017**, *53*, 13367−13370.

(35) Yuan, D.; Lu, W.; Zhao, D.; Zhou, H.-C. Highly Stable Porous Polymer Networks with Exceptionally High Gas-Uptake Capacities. *Adv. Mater.* **2011**, *23*, 3723–3725.

(36) Ma, Y.-X.; Li, Z.-J.; Wei, L.; Ding, S.-Y.; Zhang, Y.-B.; Wang, W. A Dynamic Three-Dimensional Covalent Organic Framework. *J. Am. Chem. Soc.* **2017**, *139*, 4995–4998.

(37) Chen, Y.; Shi, Z.; Wei, L.; Zhou, B.; Tan, J.; Zhou, H.-L.; Zhang, Y.-B. Guest-Dependent Dynamics in a 3D Covalent Organic Framework. *J. Am. Chem. Soc.* **2019**, *141*, 3298−3303.

(38) Gao, Z.-Z.; Wang, Z.-K.; Wei, L.; Yin, G.; Tian, J.; Liu, C.-Z.; Wang, H.; Zhang, D.-W.; Zhang, Y.-B.; Li, X.; Liu, Y.; Li, Z.-T. Water-Soluble 3D Covalent Organic Framework that Displays an Enhanced Enrichment Effect of Photosensitizers and Catalysts for the Reduction of Protons to H_2. *ACS Appl. Mater. Interfaces* **2020**, *12*, 1404−1411.

(39) Murray, J. M.; Knox, M. K.; Trueblood, C. E.; Weber, A. Potentiated state of the tropomyosin actin filament and nucleotide-containing myosin subfragment 1. *Biochemistry* **1982**, *21*, 906−915.

(40) Qi, Q.; Xi, C.-G.; Wang, H.; Zhang, D.-W.; Li, Z.-T. Stacking of bipyridinium radical cations incorporated in rigid conjugated polymers. *Supramol. Chem.* **2016**, *28*, 762−767.

(41) Muro, S.; Wiewrodt, R.; Thomas, A.; Koniaris, L.; Albelda, S. M.; Muzykantov, V. R.; Koval, M. A novel endocytic pathway induced by clustering endothelial ICAM-1 or PECAM-1. *J. Cell Sci.* **2003**, *116*, 1599−1609.

(42) Peddi, S.; Pan, X.; MacKay, J. A. Intracellular delivery of rapamycin from FKBP elastin-like polypeptides is consistent with micropinocytosis. *Front. Pharm.* **2018**, *9*, 1184.

(43) Tian, J; Yao, C.; Yang, W.-L.; Zhang, L.; Zhang, D.-W.; Wang, H.; Zhang, F.; Liu, Y.; Li, Z.-T. In situ-prepared homogeneous supramolecular organic framework drug delivery systems (sof-DDSs): Overcoming cancer multidrug resistance and controlled release. *Chin. Chem. Lett.* **2017**, *28*, 798-806.

(44) Yang, B.; Zhang, X.-D.; Li, J.; Tian, J.; Wu, Y.-P.; Yu, F.-X.; Wang, R.; Wang, H.; Zhang, D.-W.; Liu, Y.; Zhou, L.; Li, Z.-T. In Situ Loading and Delivery of Short Single- and Double-Stranded DNA by Supramolecular Organic Frameworks. *CCS Chem.* **2019**, *1*, 156–165.

(45) Fu, A.; Tang, R.; Hardie, J.; Farkas, M. E.; Rotello, V. M. Promises and Pitfalls of Intracellular Delivery of Proteins. *Bioconjugate Chem.* **2014**, *25*, 1602-1608.

(46) Lv, J.; Fan, Q.; Wang, H.; Cheng, Y. Polymers for cytosolic protein delivery. *Biomaterials* **2019**, *218*, 119358.

Table of Contents (TOC)